

# Diffusion in Metals and Intermetallics -- an Overview

H. Mehrer\*

Institut für Materialphysik, Universität Münster, Germany

## Contents

1. Introduction – some historical remarks
2. Some basics
  - 2.1 Tracer diffusion
  - 2.2 Interdiffusion
    - 2.2.2 The ‘random alloy’ approximation for interdiffusion
    - 2.2.1 Boltzmann-Matano method
  - 2.3 High-diffusivity paths in solids
  - 2.4 Diffusion mechanisms in solids
3. Self-diffusion in metals
  - 3.1 Cubic metals
  - 3.2 Uniaxial metals
  - 3.3 Metals with phase transitions
4. Impurity diffusion in metals
  - 4.1 Diffusion of substitutional impurities
  - 4.2 Slow impurity diffusion in aluminium
  - 4.3 Fast impurity diffusion in polyvalent metals
  - 4.4 Diffusion of fast diffusing interstitial impurities and of hydrogen
5. Diffusion in Intermetallics
  - 5.1 Some structures of intermetallics
  - 5.2 Influence of order-disorder transitions on diffusion



- 5.3 Diffusion in B2 phases and B2-intermetallics
- 5.4 Diffusion in  $L1_2$ -intermetallics
- 5.5 Diffusion in  $DO_3$ -intermetallics
- 5.5 Diffusion in  $L1_0$ -intermetallics
- 5.6 Diffusion in  $C11_b$ -structured molybdenum disilicide
- 5.6 Diffusion in the Laves phase  $Co_2Nb$

**Abstract:** After a few remarks about the history of diffusion in solids we remind the reader to some basics of diffusion such as tracer diffusion, interdiffusion, high-diffusivity paths, and basic diffusion mechanism in solids. We then summarize self-diffusion in cubic, hexagonal metals and metals with phase transformations. Then we summarize diffusion of substitutional impurities (solutes) in metals and remind the reader to the phenomena of slow solute diffusion in aluminium and of fast solute diffusion in polyvalent metals. We finish the part on solute diffusion with some remarks on interstitial impurities. We start the part on intermetallic alloys by reminding the reader to some of the more frequent structures. We consider examples of the influence of order-disorder transformation on diffusion. We then discuss diffusion in cubic B2-structured phases and in B2-,  $L1_2$ - and  $DO_3$ -intermetallics, We then discuss uniaxial  $L1_0$ -intermetallics and  $C11_b$ -structured molybdenum disilicide. We finish with some remarks diffusion in the cubic Laves phase  $Co_2Nb$

**Keywords:** tracer diffusion, interdiffusion, Boltzmann-Matano method, random alloy approximation, high-diffusivity path, diffusion mechanism, self-diffusion in metals, solute diffusion in metals, diffusion in cubic B2-,  $L1_2$ - and  $DO_3$ -intermetallics, diffusion in uniaxial  $L1_0$ - and in  $C11_b$  structured molybdenum disilicide. Diffusion in Laves phases

---

\*Retired Professor and Director of Institut für Materialphysik, Universität  
Münster,Germany Private  
address: Berghof 3, 73635 Obersteinenberg, Germany

## 1. Introduction – some historical remarks

Diffusion occurs in solids, gases, and liquids. It has a longstanding tradition in science. Diffusion in solids had its origin in the 19<sup>th</sup> century. It is based on the Brownian motion of atoms or molecules detected by the Scottish scientist *Robert Brown* (1773 – 1858). Brownian motion of atoms is slow in solids. Near the melting temperature of a solid a typical diffusion distance is about one micrometer per second. Near half of the melting temperature it is only about one nanometer per second.

Diffusion science is based on several corner stones. The continuum theory of diffusion originated from the work of the German scientist *Adolf Eugen Fick* (1829 - 1901) [3]. Fick was inspired by the work of the Scotsman *Thomas Graham* (1805 - 1869) on diffusion of salt in water [1]. *Albert Einstein* (1879 – 1955) realized that the basic quantity to understand Brownian motion is the mean square displacement of atoms and molecules and not their velocity. He related their mean-square displacement to the diffusion coefficient [6].

The science of diffusion in solids started with the work of the English scientist *William Chandler Roberts-Austen* (1843-1902). He studied diffusion of gold in solid lead. The values of the diffusion coefficients reported by him are in good agreement with modern values determined using a radioisotope of gold [5]. Roberts-Austen had ‘*golden hands*’ in choosing the system gold in lead for his study. Nowadays we know that diffusion of gold in lead is very fast in comparison with most other diffusion processes in solids.

The first measurements of self-diffusion in a solid were those of *Georg von Hevesy* (1885 – 1966). He studied self-diffusion in solid lead using a natural radioisotope of lead [5]. He also applied radioisotopes in biology, medicine and physics. I might mention, that one part of university hospital of Münster at the authors former university is called *von Hevesy Station*. In 1944 von Hevesy was awarded with the Nobel prize in chemistry of the year 1943 for ‘*his work on the use of tracers (radioisotopes) in the study of chemical processes.*’

Solid-state physics started with the diffraction of X-rays on crystals detected by the German *Max von Laue* (1879 - 1960), which revealed the periodic arrangement of atoms in solids. However, the perfect crystal is a ‘dead’ crystal. Solid-state diffusion and many other properties of solids require deviation from ideality. The Russian physicist *Jakov Il’ich Frenkel* (1891 - 1952) suggested that thermal agitation causes transitions of atoms from their lattice sites to interstitial positions leaving behind lattice vacancies [7]. Only a few years later, *Wagner and Schottky* [8] considered disorder with vacancies, self-interstitials and antisite defects in binary compounds. Nowadays, it is common wisdom that atomic defects are necessary as vehicles to mediate self- and solute-diffusion in solids.

A further cornerstone for diffusion in solids was provided by the American scientist *Ernest Kirkendall* (1914 – 2005). Kirkendall and coworkers studied interdiffusion (also denoted as chemical diffusion) in diffusion couples of copper and brass – a copper-zinc alloy. They observed that the plane between copper and brass moves. This plane was marked by inert markers and is nowadays called Kirkendall-plane [9]. The direction of the movement was such that one had to conclude that diffusion of Zn in brass is faster than that of copper. This was in contradiction with an at that time still common belief, that diffusion in solids occurs via direct exchange or ring mechanisms atoms. The Kirkendall effect was a strong evidence for a vacancy mechanism.

Nowadays diffusion in solids is an important topic of materials science, physical metallurgy, solid-state physics, and solid-state chemistry. In what follows, we consider diffusion in metals and intermetallics. After some basics of diffusion we provide a short overview on diffusion in pure metals and in intermetallics. Intermetallics are ordered metallic alloys.

## 2. Some basics

### 2.1 Tracer diffusion

Direct methods for studying diffusion in solids are based on the two laws of Fick and the diffusion coefficient introduced in these laws [3]. They pertain to diffusion over many interatomic distances and in this sense they are macroscopic. Fick's second law relates the concentration of atoms  $C(x,t)$ , which is a function of the position  $x$  and time  $t$ , via the diffusion coefficient  $D$  through the equation displayed in Eq. (1):

$$\frac{\partial C}{\partial t} = D \frac{\partial^2 C}{\partial x^2} . \quad (1)$$

In tracer diffusion studies of self- and solute diffusion  $D$  does not depend on the tracer concentration. This is due to the extremely small amount of tracers used in tracer experiments. Then  $D$  depends on temperature and on pressure only. Since the pioneering work of *von Hevesy* the radiotracer method is the standard technique for studies of self- and solute-diffusion in solids, provided that radioisotopes with a suitable half-life are available. The radiotracer method is highly sensitive due to the use of nuclear counting techniques. In addition it can cover a large range of diffusivities if both mechanical and sputter sectioning techniques are used for depth profiling. A further great advantage of the radiotracer method is that self-diffusion – the most basic diffusion process in a solid -- can be studied. Of course solute-diffusion can be studied as well, with radioisotopes of the solutes.

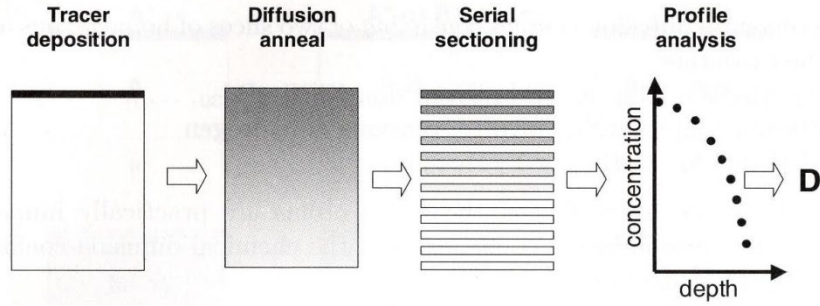


**Fig. 1** Illustration of the major steps of the tracer method for diffusion studies

A tracer experiment is schematically illustrated in Fig. 1. A thin layer of the tracer isotope ( $N$  atoms per unit area) is deposited onto a flat and polished surface of the diffusion sample. Then the concentration distribution  $C(x,t)$  at depth  $x$  of the tracer after a diffusion anneal of time  $t$  at a temperature  $T$  is described by the *thin-film solution* of Fick's second law :

$$c(x,t) = \frac{N}{\sqrt{\pi Dt}} \cdot \exp\left[-\left(\frac{x}{\sqrt{4Dt}}\right)^2\right] \quad (2)$$

The quantity  $\sqrt{Dt}$  is a typical diffusion length. The best way to measure a depth profile is serial sectioning of the diffusion sample illustrated schematically in Fig. 1 and subsequent determination of the amount of tracer per section. For radioactive tracers the specific activity per section is proportional to the tracer concentration.

Diffusion studies of very small diffusivities at low temperatures must cope with diffusion lengths in the micrometer- or submicrometer-range. Fig. 2 shows two examples of experimental penetration profiles, one for grinder sectioning and another one for sputter sectioning. Lathe or microtome sectioning is applicable for ductile samples such as pure metals or polymers. For brittle samples grinding is appropriate. In the submicrometer range sputter sectioning is a suitable sectioning technique (see, e.g. [10]).

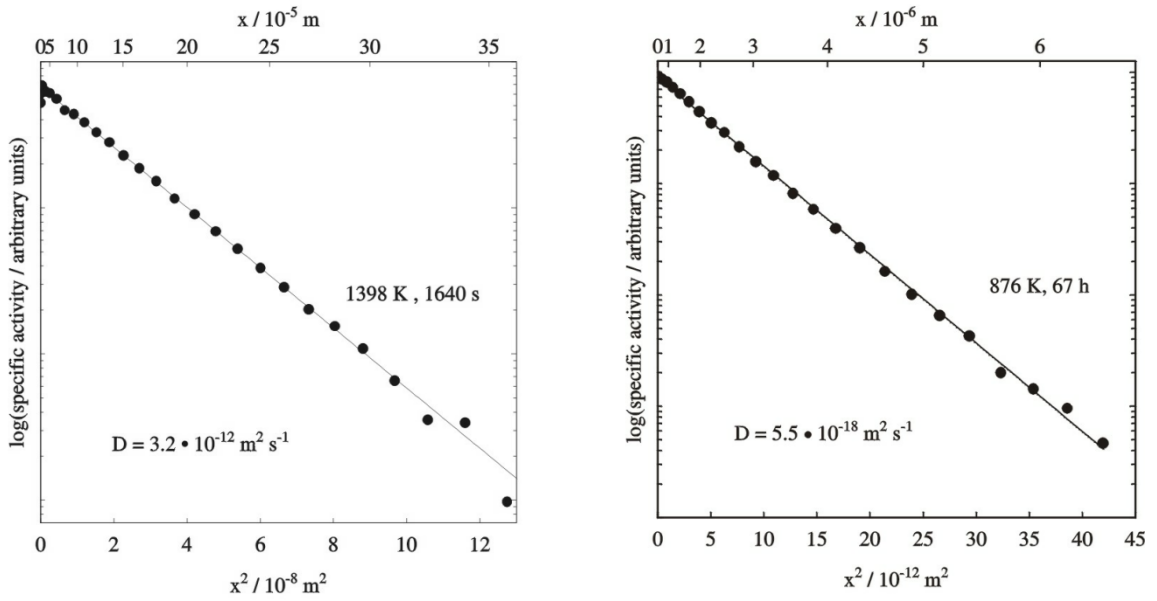


**Fig. 2** *Left*: Penetration profile of  $^{59}\text{Fe}$  in a  $\text{Fe}_3\text{Si}$  intermetallic obtained by grinder sectioning according to [13]. *Right*: Penetration profile of  $^{59}\text{Fe}$  in a  $\text{Fe}_3\text{Al}$  intermetallic obtained by sputter sectioning according to [14]. The solid lines represent fits of the thin-film solution of Fick's second law.

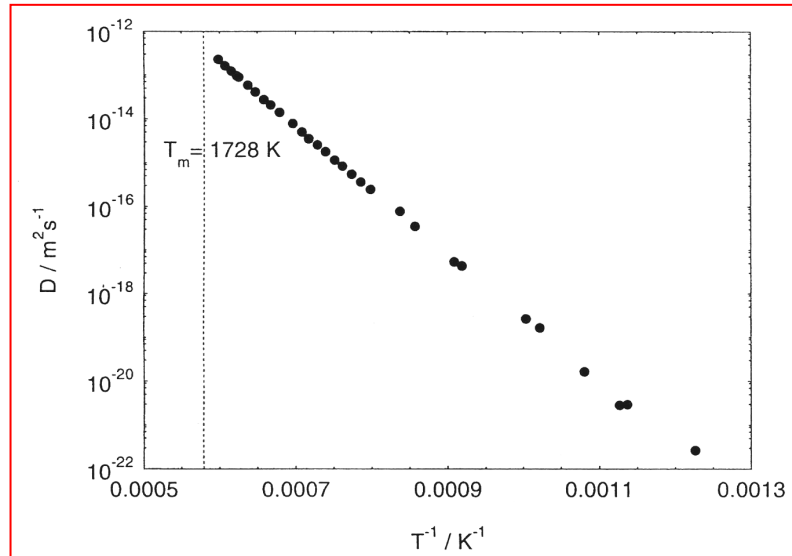


**Fig. 3** Self-diffusion in nickel monocrystals studied with a radioisotope of Ni according to [10]. Data from grinder sectioning above 1299 K are from the work of *Bakker* [27]. Data from sputter sectioning below 1200 K ( $1/T = 0.00083\text{K}^{-1}$ ) are from the work of *Maier et al.* [28].

Radiotracer diffusion studies can cover a large range of diffusion coefficients if mechanical and sputter sectioning techniques are combined. Fig. 3 displays as an example, a self-diffusion in nickel. The temperature-dependence of the diffusion coefficient can usually be described by an Arrhenius equation

$$D = D^0 \exp(-Q/kT), \quad (3)$$

using an activation enthalpy  $Q$  and a pre-exponential factor  $D^0$ .  $k$  denotes the Boltzmann constant and  $T$  the absolute temperature.

## 2.2 Interdiffusion (chemical diffusion)

For interdiffusion (chemical diffusion) studies in alloys diffusion couples are formed from two elements or from two homophase alloys with constant but different compositions. In such couples during interdiffusion the chemical composition varies in the diffusion zone. Therefore, diffusing atoms experience different chemical environments in the diffusion zone. This situation is called interdiffusion or chemical diffusion. It can be described by Fick's second law with a composition dependent interdiffusion coefficient  $\tilde{D}(C)$ :

$$\frac{\partial C}{\partial t} = \frac{\partial}{\partial x} [\tilde{D}(C) \frac{\partial C}{\partial x}]. \quad (4)$$

An interdiffusion experiment is indicated schematically in Fig. 4. The contact plane can be marked by inert markers. The shift of these markers during the diffusion annealing of the sample is called Kirkendall shift. The concentration profile can be measured for example by electron microprobe analysis. Several examples for such profiles measured on diffusion samples of Fe-Al alloys are shown in Fig. 5. These profiles can be used to determine the interdiffusion coefficient for each position. Usually, the Boltzmann-Matano method described in section 2.2.1 can be used for the analysis.

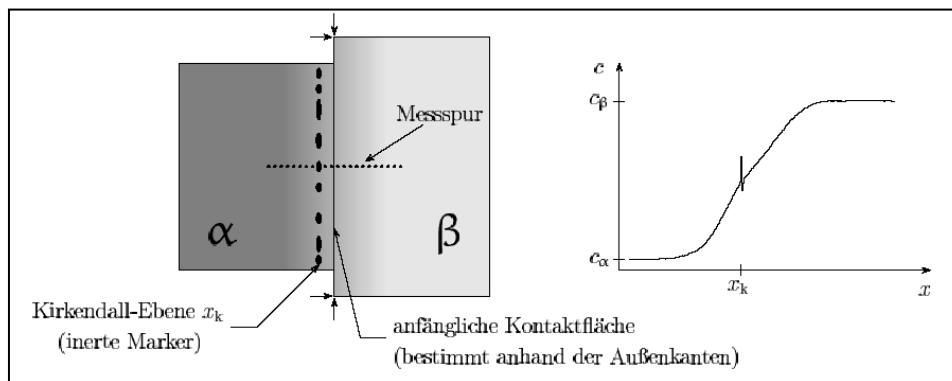


**Fig. 4** Illustration of an interdiffusion experiment between two binary alloys  $\alpha$  and  $\beta$ .  $x_k$  is the position of the Kirkendall plane.  $C_\alpha$  and  $C_\beta$  denote the initial compositions of the two alloys.

During a diffusion anneal a diffusion profile develops between the left and right concentrations  $C_L$  and  $C_R$ . The profile can be measured, e.g., by electron microprobe analysis, when the sample is cut and polished perpendicular to the initial contact plane.

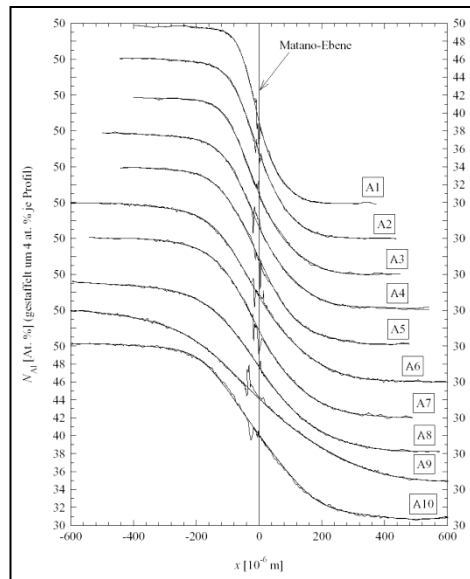


**Fig. 5** Interdiffusion profiles measured by electron microprobe analysis on Fe-Al alloy samples after diffusion anneals at ten temperatures according to *Eggersmann and Mehrer* [14].

### 2.2.1 Boltzmann-Matano method

The Boltzmann-Matano equation in terms of the quantities defined in Fig. 6 for the interdiffusion or chemical diffusion coefficient reads:

$$\tilde{D}(C^*) = -\frac{1}{2t} \int_{C_L}^{C_R} (x - x_M) dC / \left( \frac{dC}{dx} \text{ at } C^* \right) = -A^*/(2tS). \quad (5)$$

The Matano plane is obtained by choosing identical areas with horizontal dashed lines.  $A^*$  is the double-dashed area, and  $S$  denotes the slope of the profile at  $x^*$ . For more details see, e.g. [10].

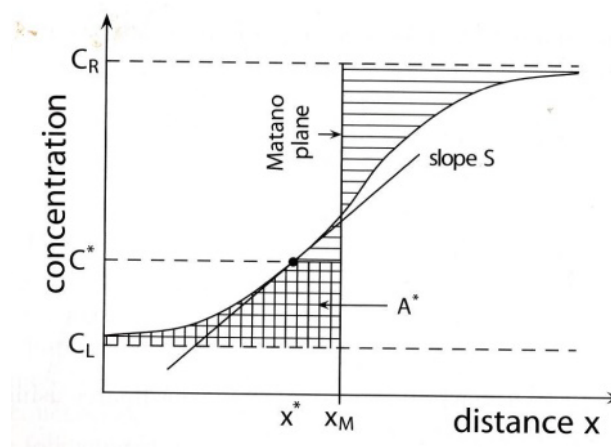


**Fig. 6** Illustration of the Boltzmann-Matano method for the determination of the interdiffusion coefficient. From [10].

### 2.2.2 The ‘random alloy’ approximation for interdiffusion

So far we have described diffusion in a binary alloy by one interdiffusion coefficient  $\tilde{D}$  which usually depends on composition. It can be deduced from an experimental concentration profile by the Boltzmann-Matano method illustrated in the previous section.

In general, the mobility of A-atoms is higher/lower than those of B-atoms. The tracer diffusivities  $D_A^*$  and  $D_B^*$  of the A- and B-atoms are different. They pertain to tracer experiments measured using A or B tracers in an A-B alloy with homogeneous composition. For relating the tracer diffusivities  $D_A^*$  and  $D_B^*$  and the interdiffusion coefficient  $\tilde{D}$  the random alloy approximation suggested by *Manning* [11] is sometimes used:

$$\tilde{D} = (N_A D_B^* + N_B D_A^*) \emptyset S . \quad (6)$$

The quantity  $\emptyset$  is the thermodynamic factor of the alloy.  $N_A$  and  $N_B$  denote the molar fractions of the A and B atoms in the alloy.  $S$  is the vacancy-wind factor:

$$S = 1 + \frac{1-f}{f} N_A N_B (D_A^* - D_B^*)^2 / (N_A D_A^* + N_B D_B^*) (N_B D_A^* + N_A D_B^*) . \quad (7)$$

Provided that one tracer diffusion coefficient and the interdiffusion coefficient have been measured, equation (6) can be used to deduce the other tracer diffusivity if the thermodynamic factor is measured or available from theoretical calculations.  $f$  is the tracer correlation factor. This procedure is sometimes helpful if for one component no suitable tracer is available,

One should however be aware that the above expression of the Manning vacancy-wind factor is an approximation. Computer simulations in simple cubic, fcc, and bcc random alloys by *Belova and Murch* [12] have shown that the Manning formalism is not accurate. It is a reasonable approximation, if the ratios of the vacancy exchange rates with A and B atoms are not too far from unity. Vacancy-wind corrections for interdiffusion in intermetallic compounds depend on the structure, the type of disorder and on the diffusion mechanism.

### 2.3 High-diffusivity paths in solids

The jump rates of atoms and hence their diffusivities along grain boundaries, dislocations and free surfaces are higher than those in the perfect crystal. This causes additional diffusion along grain boundaries, dislocation lines and surfaces. Diffusion along such high-diffusivity paths is schematically illustrated in Fig. 7.

Atomic defects discussed in the previous section are the vehicles of diffusion in the volume of a solid and are discussed in the next section.

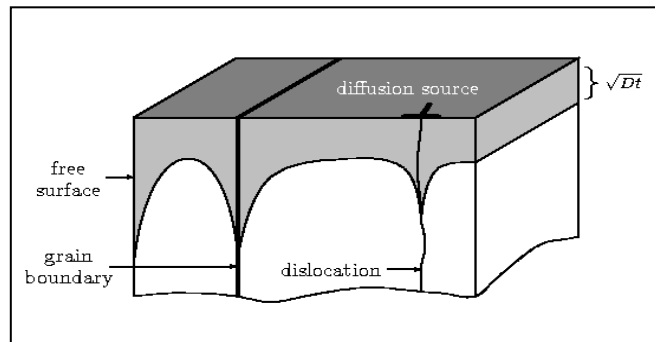


**Fig. 7** Illustration of high-diffusivity paths in a solid. From [10].

The diffusion spectrum in a solid is displayed in Fig. 8. Lattice diffusion (diffusion coefficient  $D$ ) is the slowest diffusion process. Dislocation cores (diffusion coefficient  $D_d$ ) offer smaller constraints and diffusion proceeds faster than in the lattice. Grain boundaries with their less densely packed structure enable faster atomic diffusion (diffusion coefficient  $D_{gb}$ ). Surfaces (diffusion coefficient  $D_s$ ) offer even less constraints to diffusing atoms and thus entail the highest diffusivities:

$$D < D_d < D_{gb} < D_s \quad (8)$$

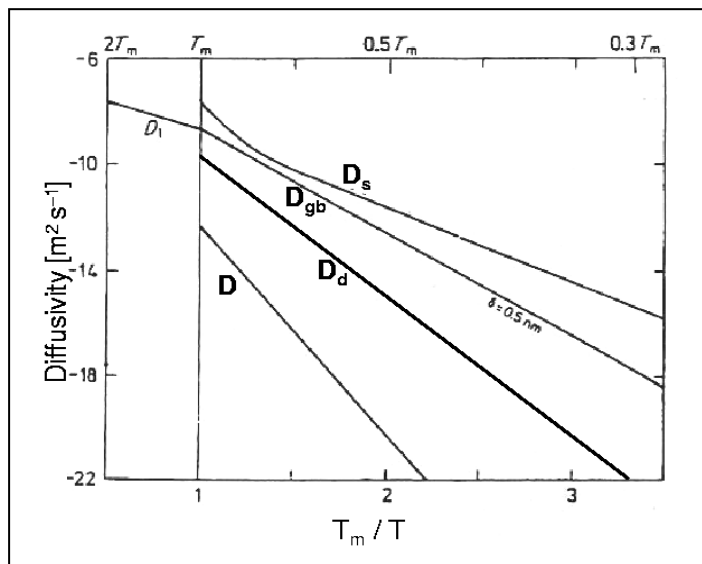


**Fig. 8** Schematic illustration of the diffusion spectrum of volume-, dislocation-, grain boundary- and surface-diffusion in a solid [10].  $T_m$  denotes the melting temperature.

## 2.4 Diffusion mechanisms in solids

Solute atoms which are considerably smaller than solvent atoms can be incorporated into interstitial sites of the host lattice. An interstitial solute diffuses by jumping from one interstitial site to a neighbouring site. The solute then diffuses by an interstitial mechanism illustrated in Fig. 9.

The most important mechanism for diffusion of matrix atoms and also for substitutional solutes in metals and many ionic crystals is the vacancy mechanism. The vacancy mechanism is illustrated in Fig. 10. In this case, atoms move through the crystal by making site exchanges with vacancies, which from time to time show up on a neighbouring site.

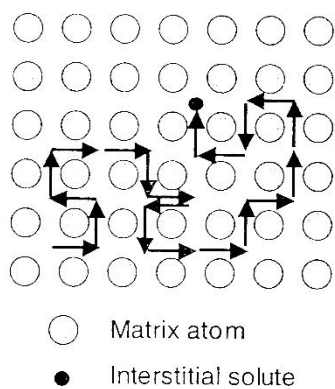


**Fig. 9** Direct interstitial mechanism.

Schematic 2D representation.

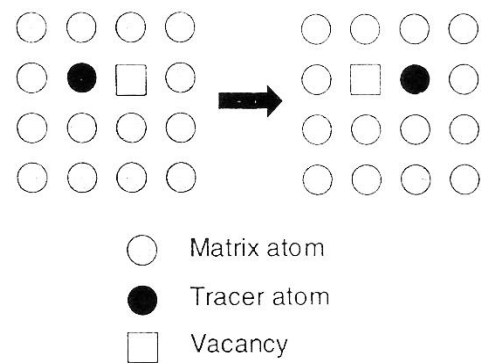


**Fig. 10** Vacancy mechanism

Schematic 2D representation.

The dominant mechanism of self-diffusion and of substitutional solutes is the vacancy mechanism. Vacancies exist in thermal equilibrium. Their site fraction in equilibrium in a monoatomic crystal is given by

$$C^{eq} = \exp(-G^F/kT). \quad (9)$$

Here  $G^F$  is the Gibbs free energy of vacancy formation, which is composed of an enthalpy  $H^F$  of vacancy formation and an entropy  $S^F$  of vacancy formation according to  $G^F = H^F - T S^F$ ,  $k$  denotes the Boltzmann constant and  $T$  the absolute temperature. Typical vacancy fractions near the melting temperature of metals are between  $10^{-3}$  and  $10^{-4}$ .

Usually there is a binding energy between vacancies, which tends to create agglomerates of vacancies such as divacancies in thermal equilibrium. The fraction of divacancies increases with temperature. In addition divacancies in metals are more mobile than monovacancies. Therefore, divacancies can also contribute to diffusion in metals especially at higher temperatures, because their

fraction increases with increasing temperature faster than that of monovacancies. The divacancy mechanism is illustrated in Fig. 11.

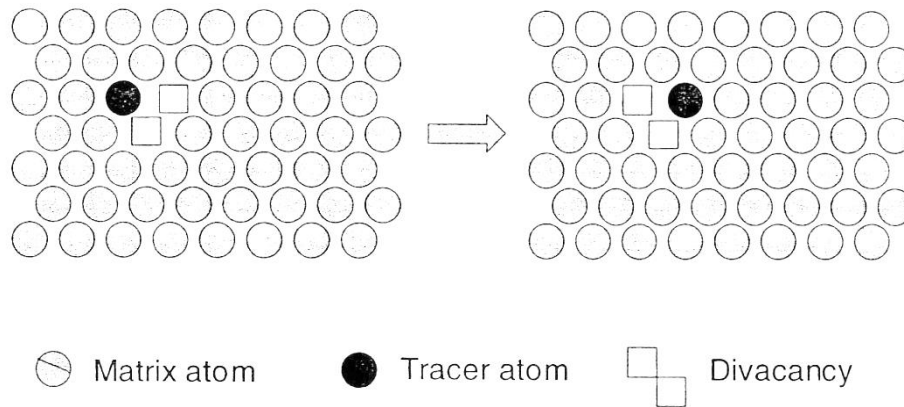


**Fig. 11** Divacancy mechanism of diffusion in a metal. Schematic 2D representation. From [10].

Semiconductors are less densely packed than metals. In semiconductors, particularly in silicon, self-interstitials, in addition to vacancies play a role as diffusion vehicles. The interstitialcy mechanism is illustrated in Fig. 12.

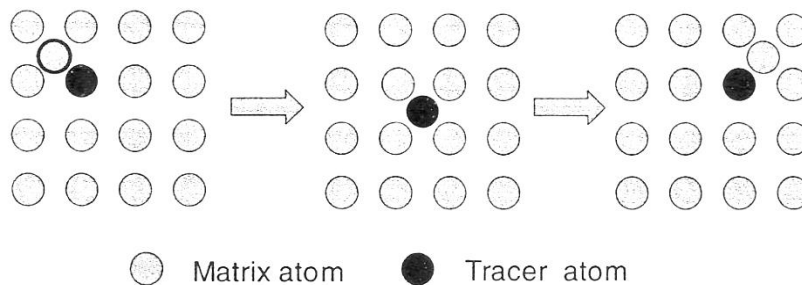


**Fig. 12** Interstitialcy mechanism or self-interstitial mechanism of diffusion (collinear jumps). Schematic 2D representation. From [10].

### 3. Self-diffusion in metals

#### 3.1 Cubic metals

Self-diffusion in metals is perhaps the best studied area of solid-state diffusion. Self-diffusion for some fcc metals is displayed in Fig. 13 as Arrhenius lines in a scale normalised with the melting temperatures. Diffusivities near the melting temperature lie between  $10^{-12} \text{ m}^2\text{s}^{-1}$  and  $10^{-13} \text{ m}^2\text{s}^{-1}$ . An exception is the group IV metal lead, where the diffusivity is about one order of magnitude lower.

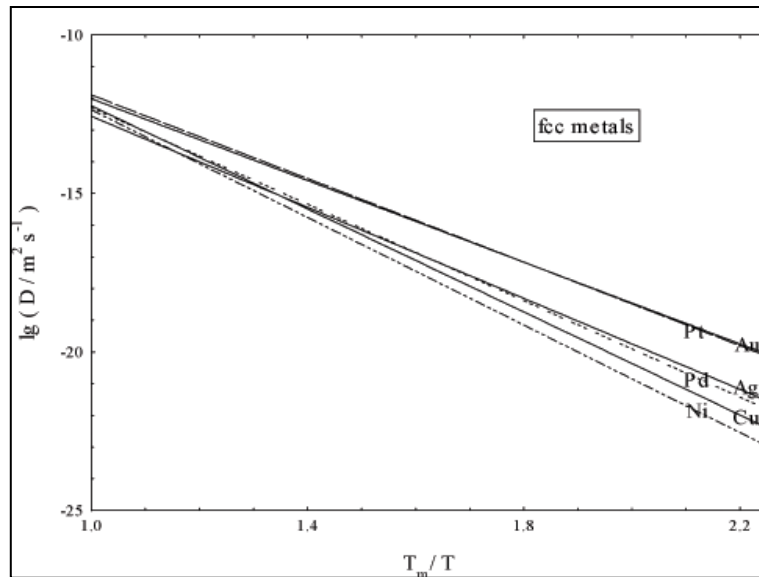


**Fig. 13** Self-diffusion of fcc metals in a temperature scale normalized with the melting temperature  $T_m$  according to [15].

Self-diffusion in a normalized temperature scale for several bcc metals is shown in Fig. 14. Diffusivities near the melting temperature lie between  $10^{-11} m^2 s^{-1}$  and  $10^{-12} m^2 s^{-1}$ . These values are about one order of magnitude higher than in fcc metals. The diffusion ‘spectrum’ of bcc metals is wider than for fcc metals. Self-diffusion in the normalized scale is slowest for group VI transition metals Cr, Mo, and W and fastest for alkali metals. A common feature of fcc and bcc metals is that within one group of the periodic table self-diffusion at the same homologous temperature is slowest for the lightest metal and fastest for the heaviest metal.

Self-diffusion in metals is dominated by the monovacancy mechanism at temperature below  $2/3 T_m$ . At higher temperatures a divacancy contribution, which varies from metal to metal plays an additional role. For details see [10].

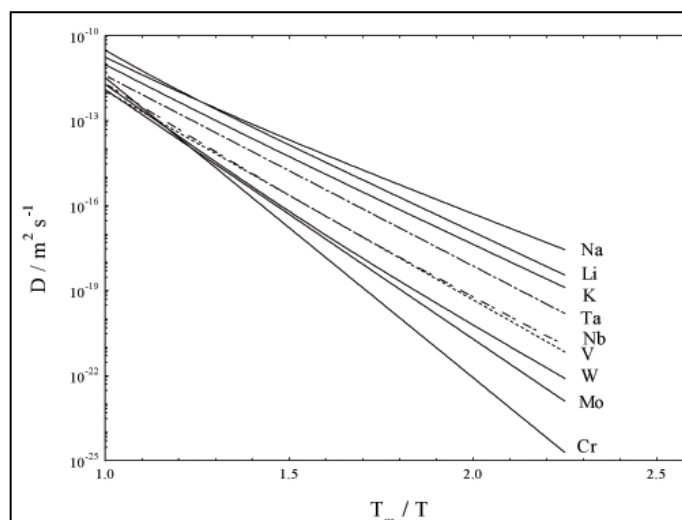


**Fig. 14** Self-diffusion of bcc metals in a temperature scale normalized with the melting temperatures  $T_m$ . From [10], according to [15].

### 3.2 Uniaxial metals

Several metals are uniaxial. Zn, Cd, Mg, and Be crystallize in the hexagonal close-packed structure. A few others such as In and Sn are tetragonal. In tracer experiments with oriented monocrystals the diffusion coefficients in the two principal directions, parallel and perpendicular to the hexagonal or tetragonal axes, can be determined. Fig. 15 displays tracer self-diffusion of Zn, In, and Sn for both principal directions.

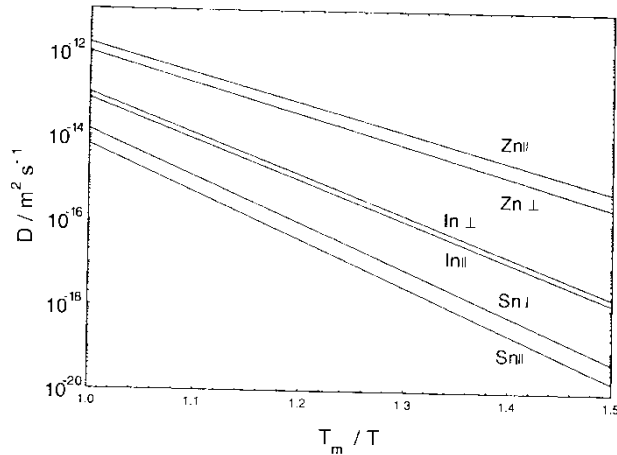


**Fig. 15** Self-diffusion of uniaxial metals Zn, In, and Cd parallel and perpendicular to their axes a temperature scale normalized with the melting temperature  $T_m$ . From [10].

### 3.3 Metals with phase transitions

Some metals undergo phase transformations and exist in different crystalline structures in different temperature regions. Iron is a famous example.  $\alpha$  –iron is bcc,  $\gamma$  –iron is fcc, and  $\delta$  –iron is again bcc. Below the Curie temperature  $T_C = 1043$  K iron is ferromagnetic. Self-diffusion in iron is shown in Fig. 16.

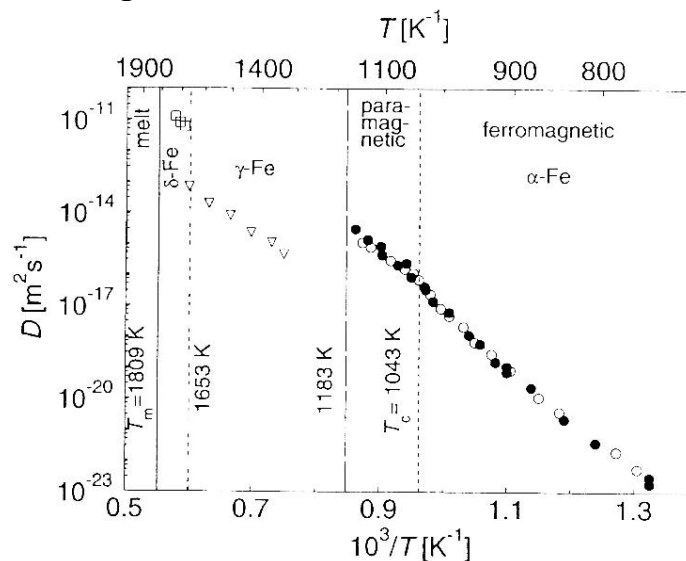


**Fig. 16** Self-diffusion in the three phases  $\alpha$  –,  $\beta$  –and  $\delta$ – iron. From [10].

Group IV transition metals undergo a transition from an hcp low-temperature phase to a bcc high-temperature phase. An Arrhenius diagram for self-diffusion in titanium is shown in Fig. 17. Upon the transition from the  $\alpha$ - to the  $\beta$ - phase, the diffusivity increases by about 3 orders of magnitude.

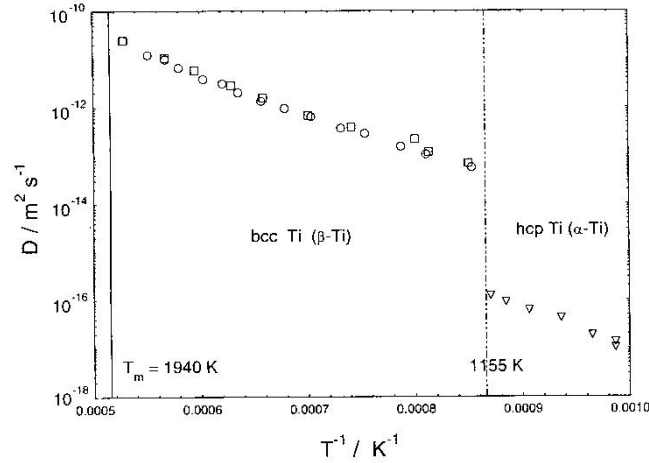


**Fig. 17** Self-diffusion in the  $\alpha$ - and  $\beta$ -phases of titanium [10].

A common feature of Figs. 16 and 17 is that diffusion in the denser packed phases is slower than in the more open bcc phase.

## 4, Impurity diffusion in metals

### 4.1 Diffusion of substitutional impurities

In this section we consider tracer diffusion of substitutional solutes (impurities) in an otherwise pure metal. Substitutional impurities are located in regular lattice sites of the crystal. Fig. 18 displays impurity diffusion in gold and in silver together with self-diffusion. Impurity diffusion coefficients  $D_i$  and self-diffusion coefficients  $D$  reveal the following features of substitutional impurities:

$$1/100 \leq D_i/D \leq 100. \quad (10)$$

The activation enthalpies of impurity and self-diffusion,  $Q_i$  and  $Q$ , are not much different:

$$0.75 \leq Q_i/Q \leq 1.25. \quad (11)$$

Diffusion of substitutional impurities in the other fcc metals Cu and Ni and in the hcp metals Zn and Cd obey similar limits.

There are however exceptions from this behaviour, which concern extremely fast or very slow diffusion. These cases will be considered in the next two subsections.

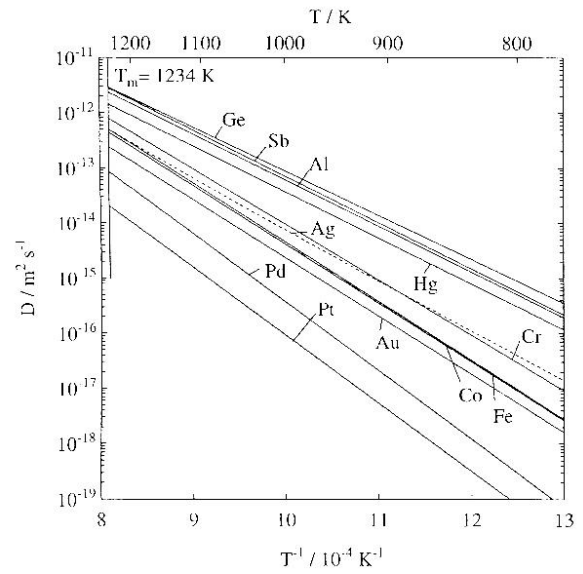
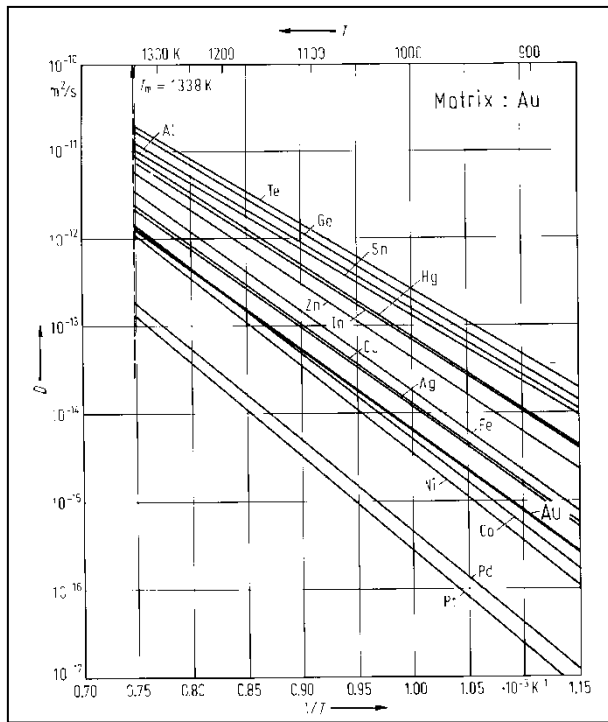


**Fig. 18** Diffusion of substitutional impurities in gold (left) [13] and in silver (right) [10].

#### 4.2 Slow impurity diffusion in aluminium

Aluminium like the noble metals crystallizes in the fcc structure. In contrast to the noble metals it is trivalent. Diffusion of impurities in aluminium is different from impurities in noble metals, which can be seen in Fig. 19.

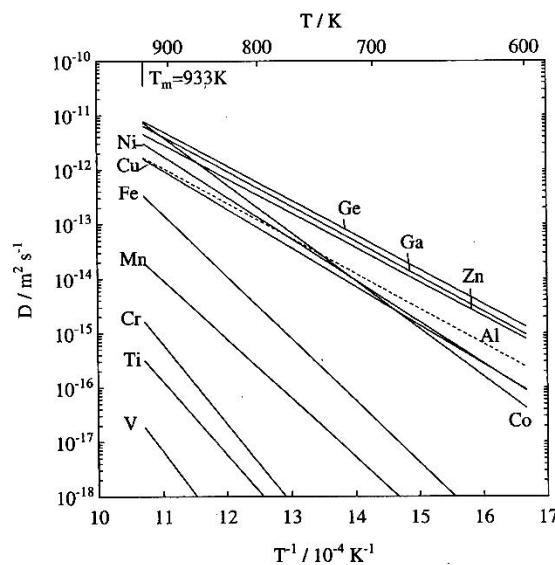


**Fig. 19** Impurity diffusion in Al and self-diffusion (dashed line) [10].

A striking feature of impurity diffusion in aluminium is that most transition metals are extremely slow diffusers compared to Al self-diffusion. In contrast non-transition elements have diffusivities slightly higher than Al self-diffusion.

### 4.3 Fast impurity diffusion in polyvalent metals

The fast diffusion of gold in lead, detected by *Roberts-Austen*, was already mentioned in the introduction. Fig. 20 shows an Arrhenius diagram of impurities in lead together with self-diffusion of lead (dashed line) according to [10].

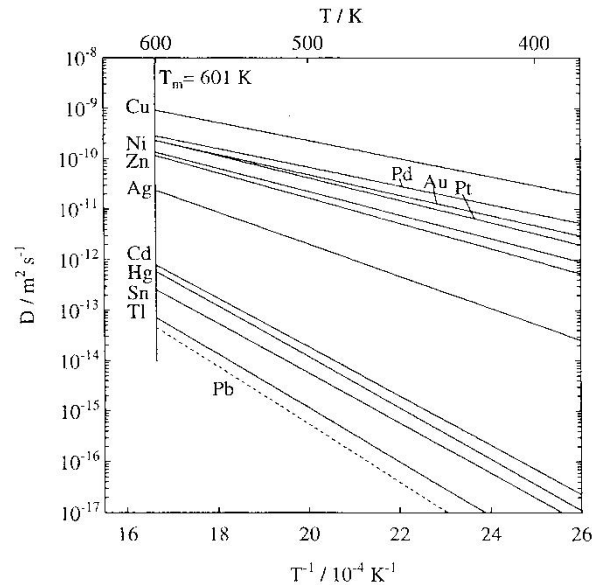


**Fig. 20** Impurity diffusion in lead and self-diffusion of lead (dashed line) [10].

Some impurities, such as Sn, Ti, Hg, and Cd show ‘normal’ impurity diffusion behaviour. However, Cu, Ag, Au, Zn, and Ni group metals have diffusivities several orders of magnitude faster than self-diffusion. Fast diffusion of 3d-metals is also observed in some other polyvalent metals such as In, Sn, Ti, Zr, and Hf.

Fast impurity diffusion in polyvalent metals is thought to be exceptional, because the diffusivities lie far above the range expected for a vacancy mechanism. On the other hand, the relatively large atomic radii of these impurities seem to exclude dissolution predominantly on interstitial sites. The fast diffusion of such impurities is attributed to the *dissociative mechanism*. Dissociative diffusion implies that the impurity is mainly dissolved on substitutional sites but a small fraction can be dissolved in interstitial sites of the host crystal. The impurities on interstitial site have a high mobility. For details about the dissociative mechanism we refer to the author’s textbook [10].

### 4.4 Diffusion of fast diffusing interstitial impurities and of hydrogen

Interstitial atoms diffuse much faster than substitutional solutes and atoms of the solvent itself. The small sizes of interstitial solutes permit fairly easy jumping between neighbouring interstitial sites. Typical examples are displayed in Fig. 21, where the diffusion coefficients of C, O, and N in niobium are shown together with Nb self-diffusion. The activation enthalpies of the interstitial diffusers are much smaller than that of Nb self-diffusion. Interstitial diffusivities can be as high as diffusivities in liquids, which are near the melting temperature typically between  $10^{-8}m^2/s$  and  $10^{-9}m^2/s$ .

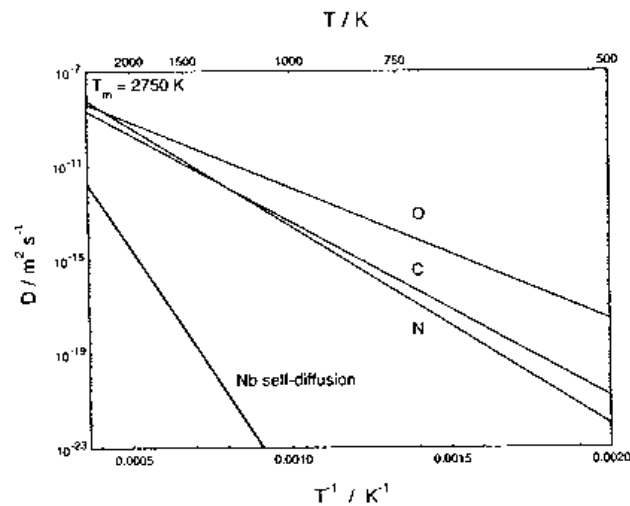


**Fig. 21** Diffusion of interstitial solutes C, N, and O in niobium. Niobium self-diffusion is shown for comparison [10].

Hydrogen forms interstitial solutions with most metallic elements. Some metals have a high solubility for hydrogen (Ti, Zr, Hf, Nb, Ta, Pd, ...) and form hydrides at higher concentrations. Other metals have a low solubility. Examples with low solubility are Fe, Co, Ni, noble metals, group VI and group VII metals.

In addition hydrogen has a small mass. As a consequence quantum effects can be expected in its diffusion behaviour. For example, H and D in Nb have different activation enthalpies. In addition the three available hydrogen isotopes (H, D, T) have large mass ratios, which permit studies of isotope effects. We consider below two examples with low hydrogen concentration. For further details we refer the reader to the author's textbook [10] and further references therein. Fig. 22 displays diffusion of hydrogen in Fe, Pd, and Ni.

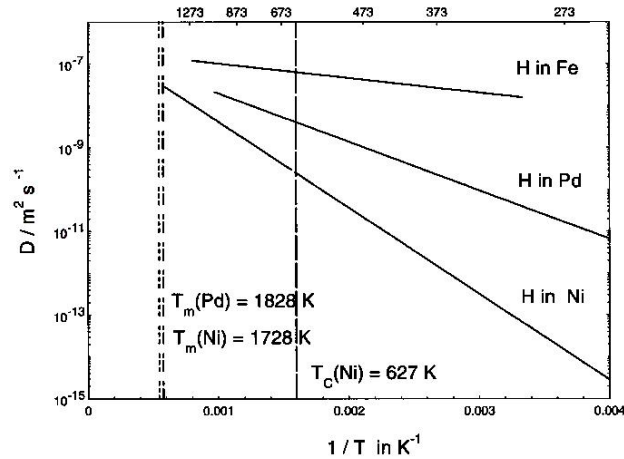


**Fig. 22** Diffusion of H in Ni, Pd and Fe. From [10] according to *Alefeld and Völkl* [16].

The data for H in Ni cover about seven orders of magnitude of the diffusion coefficient. Nickel has a magnetic transition with a Curie-temperature at 627 K. The Arrhenius parameters below and above the Curie temperature are only slightly different. The system Pd-hydrogen has been studied by several experimental methods with remarkable consistency. Diffusion of hydrogen in iron has attracted a lot of interest due to the technical challenge of hydrogen embrittlement of iron and steels. The values of hydrogen diffusivity are higher in Fe than in the closer packed metals Ni and Pd.

## 5. Diffusion in intermetallics

### 5.1 Some structures of intermetallics

Intermetallics are compounds of metals or of metals and semimetals. The structures of intermetallics are different from those of their constituents. Three frequent cubic structures of intermetallics are shown in Fig. 23.

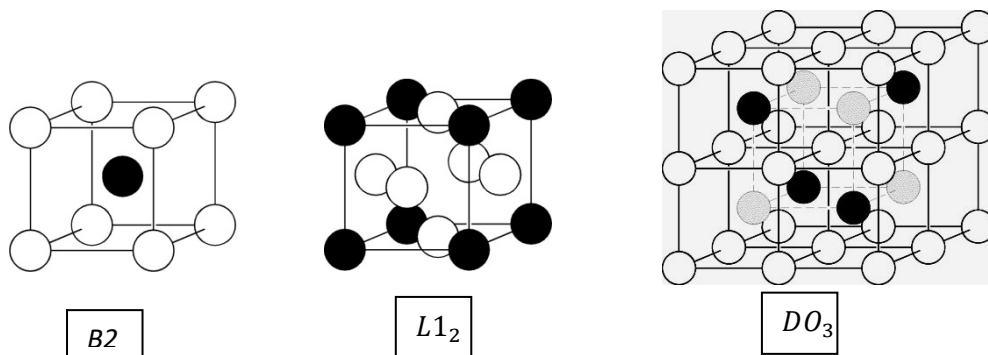


**Fig. 23** Ordered structures of three cubic intermetallic alloys:  $B2$  (left),  $L1_2$  (middle),  $DO_3$  (right). Open circles: a-atoms. Full circles: B-atoms

Examples for intermetallics with  $B2$  structure are FeAl, CoAl, NiAl, CoGa, CuZn, AuZn and AuCd. The  $L1_2$ -structure is also called  $Cu_3Au$  structure. Further examples for this structure are  $Ni_3Al$ ,  $Ni_3Ga$ , and  $Ni_3Ge$ . The prototype  $Cu_3Au$  shows  $L1_2$ -order at temperatures below 600 K, above 600 K it is disordered. An example for the  $DO_3$  structure is  $Fe_3Si$ .

## 5.2 Influence of order-disorder transitions on diffusion

Order-disorder alloys reveal an ordered arrangement (here  $B2$ ) of atoms at low temperature, which becomes progressively disordered with increasing temperature. At a critical temperature long range order disappears. The influence of such a transition on self-diffusion of both components is well documented for the Cu-Zn system, which has been studied by *Kuper et al.* [17]. Fig. 24 shows self-diffusion of both components in CuZn according to [17]. Below the critical temperature CuZn crystallizes in  $B2$  order, above it is disordered.

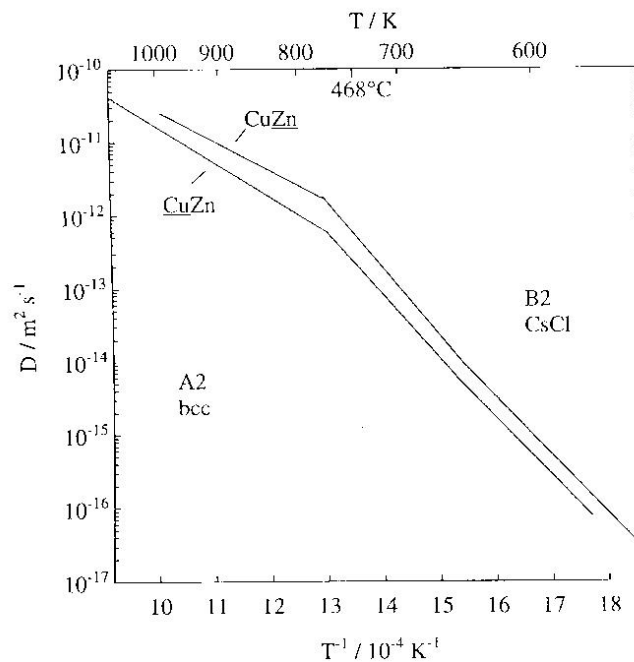


**Fig. 24** Self-diffusion of  $^{64}Cu$  and  $^{65}Zn$  radiotracers in CuZn, From [10] according to *Kuper et al.* [17]. The diffusing component is underlined.

The influence at the order-disorder transition at 468 °C on diffusion of both components causes a change in the slope of the Arrhenius plot. The slope of both components obey the inequality

$$Q_{B2} > Q_{A2} . \quad (11)$$

The activation energy is higher for the structure with the higher order. The disordered high-temperature phase has a lower activation enthalpy.

### 5.3 Diffusion in B2 phases and B2 intermetallics

Much of the diffusion work on intermetallics is devoted to *B2* phases. Fig. 25 summarizes self-diffusion in several *B2* structured intermetallics. A fairly general feature is that for most of these alloys the ratio between the diffusivities of the components is not much different from unity. This ‘*coupling*’ indicates that diffusion of both components is mediated by the same defect.

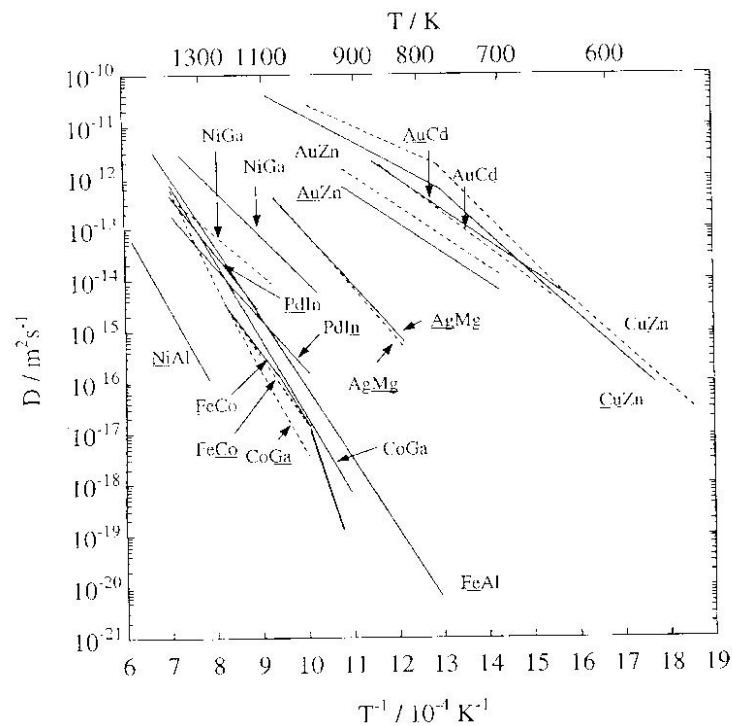


**Fig. 25** Self-diffusion of components in *B2* structured intermetallics. The diffusing components are underlined [10].

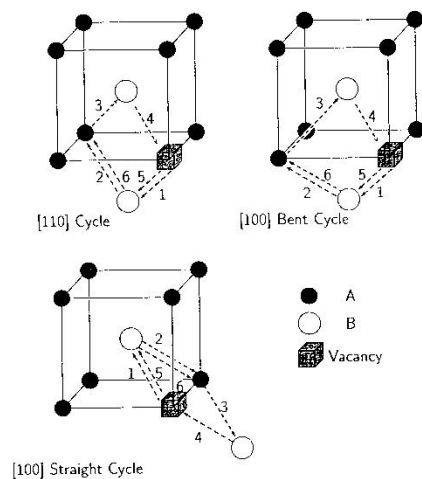


**Fig. 26** Illustration of the six-jump vacancy cycle (6JC) in the  $B2$  structure. The arrows indicate vacancy jumps, the numbers indicate the jump sequence. From [10].

Several order-retaining mechanisms, for which diffusion is ‘*coupled*’ have been proposed for  $B2$  structured intermetallics. We mention here only the six-jump-cycle mechanism (6JC) illustrated in Fig. 26. In a highly ordered state the ratio of the diffusivities for the 6JC mechanism lie within narrow limits between about  $\frac{1}{2}$  and 2. If the chemical composition deviates from the stoichiometric one and as disorder increases with temperature interactions with antisite atoms widens these limits. Triple defect mechanism, anti-structure bridge mechanism, and vacancy pair mechanism have also been proposed. For further details see, e.g. [10].

#### 5.4 Diffusion in $L1_2$ intermetallics

In a completely ordered, stoichiometric  $L1_2$  structured compound  $A_3B$ , each A atom is surrounded by 8 A-atoms on nearest neighbour sites and 4 B- atoms on second nearest neighbour sites (see Fig. 23). Hence the sublattice of the majority atoms is interconnected by nearest-neighbour bonds. Diffusion in some  $L1_2$  intermetallics is displayed in Fig. 27.

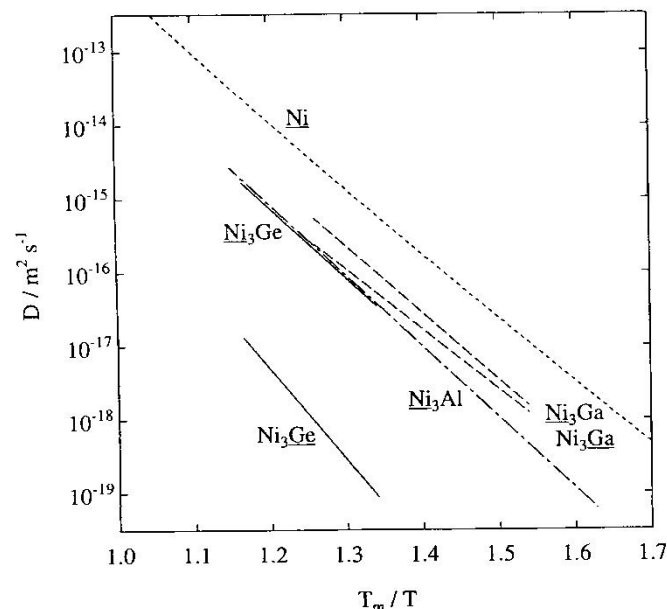


**Fig. 27** Self-diffusion in three  $L1_2$  intermetallics  $Ni_3Al$ ,  $Ni_3Ga$ ,  $Ni_3Ge$ . The diffusing components are underlined. The temperature scale is normalised to the pertaining melting temperature. Ni self-diffusion is also shown for comparison [10].

Fig. 27 shows that the diffusivities of the minority elements can vary from very different to very similar of those of the majority elements. The diffusivity of Ge in  $Ni_3Ge$  is considerably lower than that of Ni, on the other hand for  $Ni_3Ga$  the diffusivities for Ni and Ga are quite similar

Perhaps the most important and best known  $L1_2$  intermetallic is  $Ni_3Al$ . It is used as strengthening phase in Ni-base superalloys. The phasefield of  $Ni_3Al$  in the Ni-Al system exists on both sides of the stoichiometric composition, but it is fairly narrow. Diffusion of both components is displayed in Fig. 28. Ni diffusion has been studied using the radiotracer method. Interdiffusion studies in combination with the Boltzmann-Matano method were used to deduce Al diffusion coefficients, because a suitable Al tracer does not exist.

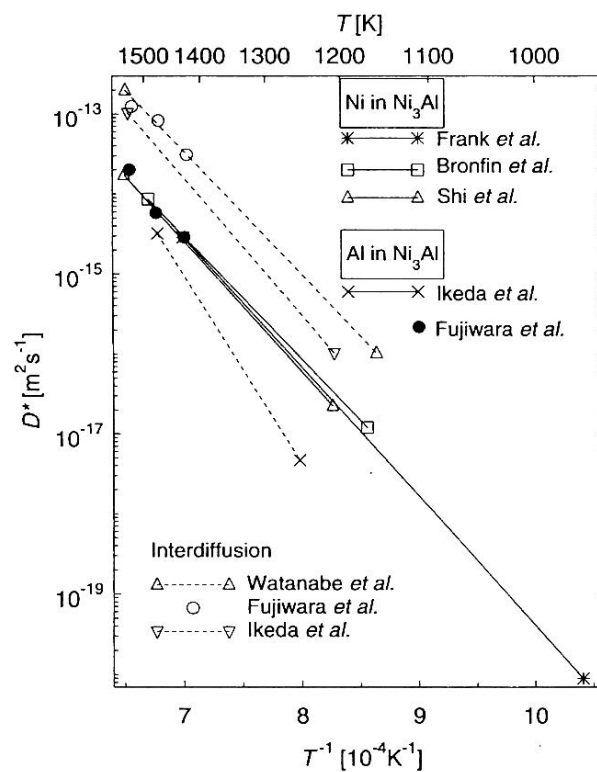


**Fig. 28** Self-diffusion of Ni and Al in  $L1_2$  structured  $Ni_3Al$ . From [10] according to *Herzig and Divinski* [18].

The data of Fig. 28 indicate that the diffusion coefficients of Ni and Al are not much different. It is quite natural that diffusion of the majority component in  $L1_2$  intermetallics occurs by a sublattice vacancy mechanism. The diffusion mechanism of the minority elements is less obvious. The diffusion coefficient of Ge in  $Ni_3Ge$  is very low, whereas the diffusivities of Ga and of Al in their compounds are not much different from those of the major components. Minority components in  $L1_2$  intermetallics most likely diffuse as antisite atoms in the majority sublattice. For some details, see e.g. [10] and further references cited therein.

## 5.5 Diffusion in $DO_3$ intermetallics

The majority sublattice of A atoms in  $DO_3$  intermetallics, like in the  $L1_2$  structure, is interconnected by nearest neighbour bonds. This is not the case for the B-sublattice (see Fig. 23). Thus an A-atom can diffuse by nearest neighbour jumps in its own sublattice. If a B-atom would jump to a nearest neighbour in the B-sublattice it had to perform a third-nearest neighbour jump with respect to the bcc unit cell. An alternative for the diffusion of B-atoms is a nearest neighbour jump into the A-sublattice. Thereby it will form a B antisite defect in the A-sublattice. Then the B-atom could diffuse as a kind of ‘*impurity*’ in the A-sublattice. Both options, third-nearest neighbour jumps or antisite formation, requires a higher activation enthalpy for B-atoms as compared to sublattice diffusion of A-atoms. This would entail a lower diffusivity for B-atoms

Fig. 29 shows an Arrhenius plot of Fe- and Ge-diffusion in three compositions of  $Fe_3Si$  according to *Gude and Mehrer* [19]. The data cover temperature ranges mostly within the  $DO_3$  phasefield. One difficult experiment with the very short-lived isotope  $^{31}Si$  (half-life 2.6 hours) showed that Ge and Si in  $Fe_3Si$  diffuse indeed at very similar rates. A slight influence of the paramagnetic-ferromagnetic transitions for the two alloys with higher Fe content can be seen in Fig. 29.

Diffusion for all three compositions shows that diffusion of the majority component Fe is significantly faster than Ge or Si diffusion. Another feature of Fig. 29 is that Fe-diffusion increases with increasing Si-content. This observation is supported by positron annihilation studies [20]. These experiments show that the increase of the Fe diffusivity is accompanied by an increase of the content of thermal vacancies in  $Fe_3Si$ .

In addition Mößbauer experiments on  $Fe_3Si$  by *Sepiol and Vogl* [21] have shown that the atomic jump vectors of Fe-atoms are in agreement with nearest-neighbour jumps in the Fe-sublattice. These findings clearly support a sublattice vacancy mechanism for Fe-diffusion.

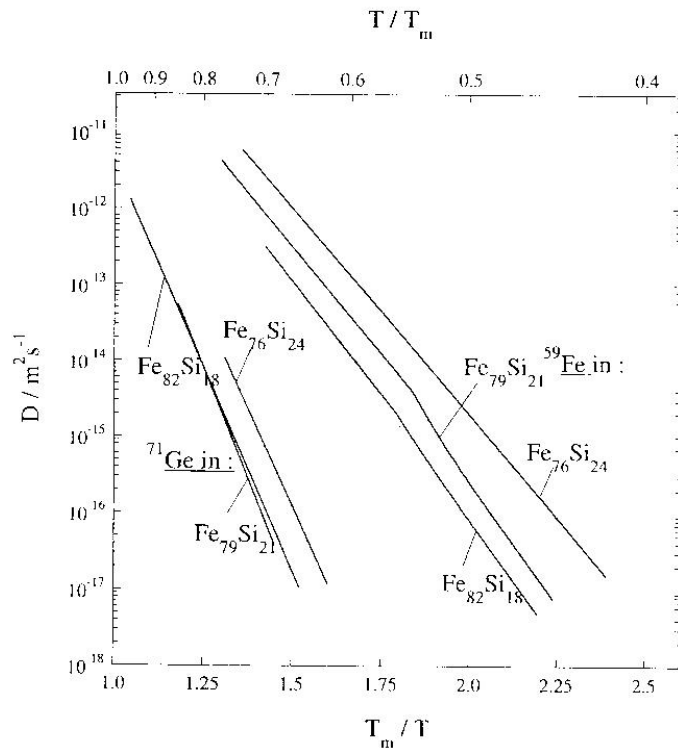


**Fig. 29** Fe self-diffusion and Ge solute diffusion in three compositions of the  $DO_3$  phase  $Fe_3Si$ . The temperature scales are normalized with the corresponding liquidus temperatures. From [10], according to *Gude and Mehrer* [19].

For the  $DO_3$  phase of  $Cu_3Sn$  like in the case of  $Fe_3Si$  diffusion of the majority component is significantly faster than that of the minority component.

### 5.5 Diffusion in $L1_0$ intermetallics

As shown in Fig. 30 the  $L1_0$  structure is tetragonal with the approximate composition AB. It is also called CuAu structure. It can be derived from an ordered fcc structure with A and B atoms sequentially occupying (001) planes with a slight tetragonal distortion in [001] direction. An example of technological interest is  $\gamma$ -TiAl. It is of interest for structural applications. The intermetallics NiPt, FePt, CoPt, FePd, and NiMn are of interest for magnetic applications.

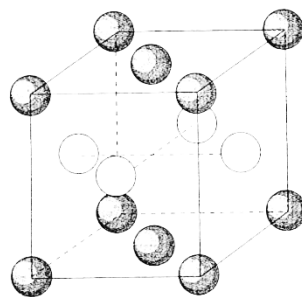


**Fig. 30**  $L1_0$  structure of some intermetallics. From [10]

The tracer diffusivities of  $^{44}\text{Ti}$  and of Ga and In in  $\gamma\text{-TiAl}$  have been studied parallel and perpendicular to the principal axes and are displayed in Fig. 31. In and Ga are isoelectronic to Al and were used to simulate Al diffusion,

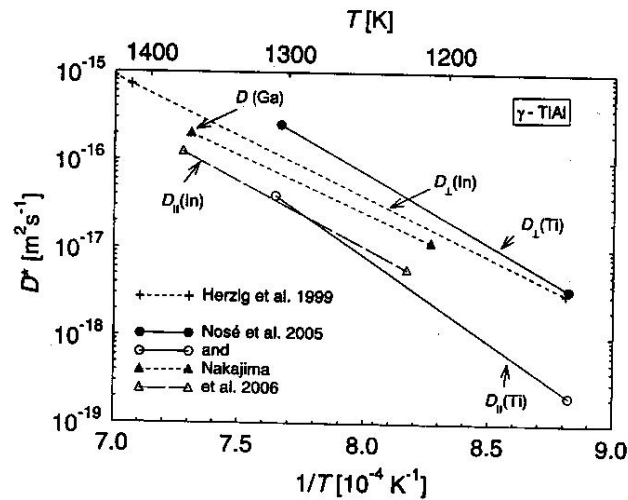


**Fig. 31** Diffusion in  $\gamma\text{-TiAl}$ . Ti and In was studied on mono- crystals parallel and perpendicular to the principal axes. Ga diffusion was studied in polycrystals. From [10].

Ti and In diffusion is faster perpendicular to the tetragonal axis than parallel to it. For Ti the anisotropy is almost one order of magnitude, whereas for In it is slightly smaller. Diffusion within the close-packed layers of the same type of atoms is faster than perpendicular to it.

Self-diffusion of Ni and Mn tracers have been studied in equiatomic polycrystalline NiMn alloys by *Peteline et al.* [22]. The results are displayed in Fig. 32. The phase diagram of Ni-Mn shows that equiatomic NiMn occurs in three different crystal structures. At temperatures below 1000 K the  $L1_0$  structure is reported. Between 1000 K and 1180 K the B2 order forms, and between 1180 K and the melting temperature NiMn is a disordered fcc alloy.

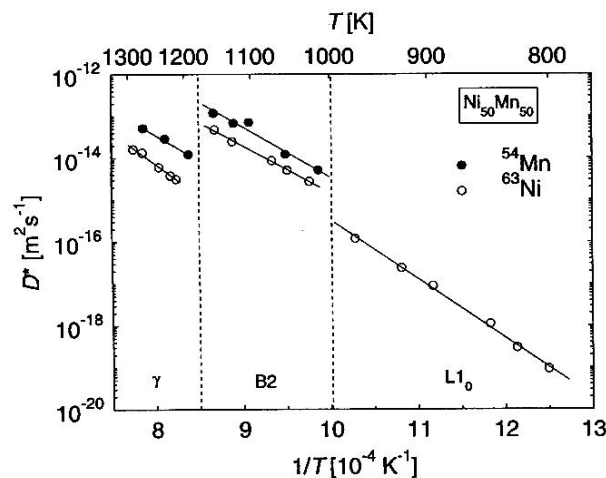


**Fig. 32** Self-diffusion of Mn and Ni in polycrystalline NiMn. From [10] according to *Peteline et al.* [22]-

The Ni diffusivity in the low temperature is about one order of magnitude lower than in the  $B2$  structured phase. The two high-temperature phases are both cubic and thus not anisotropic. The high-temperature fcc phase is more densely packed than the  $B2$ -phase, Therefore the diffusivity decreases at the transition temperature 1180 K. Since the experiments were performed on polycrystals nothing can be said about a possible diffusion anisotropy in the low temperature phase.

## 5.6 Diffusion in $C11_b$ structured molybdenum disilicide

Molybdenum disilicide ( $\text{MoSi}_2$ ) crystallizes in the  $C11_b$  structure shown in Fig. 33. It is a highly stoichiometric compound with a very high melting temperature at 2030 °C.  $\text{MoSi}_2$  is a widespread high-temperature material for structural applications in aircrafts, cars, gas-turbines, ignition-plugs. ... It is also a frequent material for heating elements in high temperature furnaces. It has good electrical properties and an excellent oxidation resistance.

The tetragonal unit cell of the  $C11_b$  structure is shown in Fig. 33. The structure is a sequential stacking of one Mo and two Si layers. Each molybdenum atom is somehow ‘encaged’ by 8 silicon atoms.

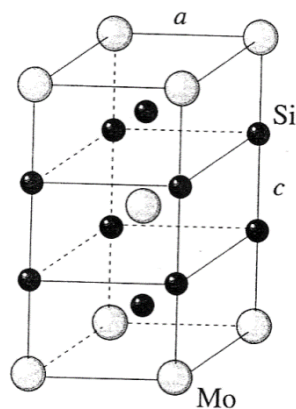


**Fig. 33** Unit cell of molybdenum disilicide  $\text{MoSi}_2$ . Full circles are Mo atoms.

A tetragonal crystal has two principal diffusivities. Therefore diffusivities parallel and perpendicular the axes need to be considered for self-diffusion as well as for solute diffusion.

Diffusion of  $^{31}\text{Si}$ ,  $^{71}\text{Ge}$ - and  $^{99}\text{Mo}$  tracers has been measured on  $\text{MoSi}_2$  monocrystals in both principal directions by *Salamon et al.* [23, 24]. The results are displayed in Fig. 34. Si diffusion in both principal directions is many orders of magnitude faster than molybdenum diffusion and the activation enthalpies of silicon diffusion are smaller than those of molybdenum diffusion. This large diffusion asymmetry between the two components suggests that the components diffuse in their own sublattice.

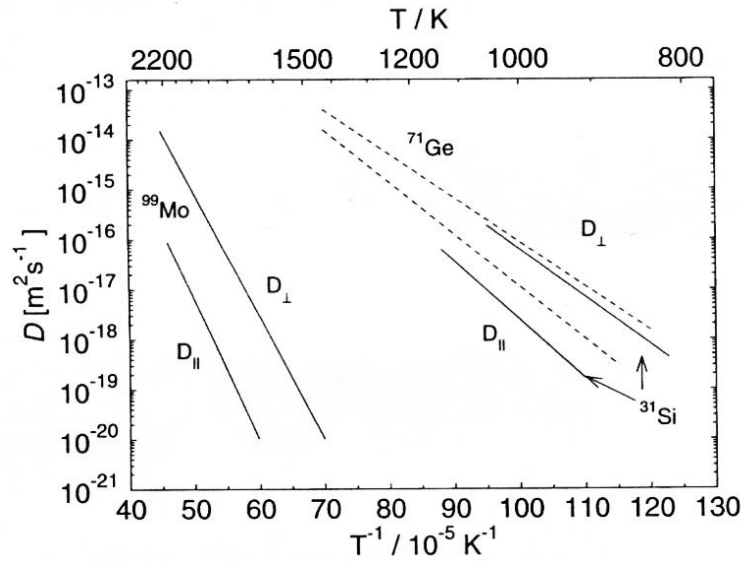


**Fig. 34** Diffusion of Mo, Si and Ge along both principal axes of MoSi<sub>2</sub> monocystals. From [10] according to *Salamon et al.* [23, 24].

Diffusion in MoSi<sub>2</sub> also reveals a large diffusion anisotropy between the major crystal directions.

Positron annihilation studies indicate that thermal vacancies form in the Si-sublattice of MoSi<sub>2</sub>. This observation and the large diffusion asymmetry between Si and Mo diffusion suggest that diffusion in the Si sublattice occurs via thermal vacancies.

## 5.6 Diffusion in the Laves phase Co<sub>2</sub>Nb

Laves phases are a numerous group of intermetallics. More than 360 binary Laves phases are known and even more ternary ones. They form if the component radii have a ratio of about 1.25. This ratio permits high packing density at an approximate composition of B<sub>2</sub>A. There are three related structures: *C15* (cubic, also called Mg<sub>2</sub>Cu-type), *C14* (hexagonal), and *C26* (also hexagonal). The cubic *C15* type structure is illustrated in Fig. 35.

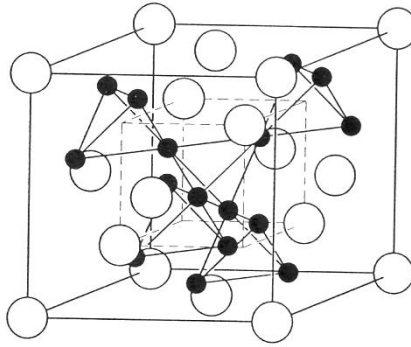


**Fig. 35** Unit cell of the cubic *C15* Laves phase  $\text{Co}_2\text{Nb}$ . Full circles represent Co atoms, open circles represent Nb atoms.

Information about diffusion in Laves phases are very scarce [15]. The only tracer diffusion study known to the author is available for the cubic Laves phase  $\text{Co}_2\text{Nb}$  by *Denkinger and Mehrer* [28]. The results are shown in Fig. 36. Co diffusion was studied for two compositions which both lie inside the phasefield of the *C15* phase. Nb diffusion was studied for the Co leaner composition only.

Diffusion of the majority component Co is significantly faster than diffusion of the minority component Nb. Similarities between the  $L1_2$  phases, which are also close-packed structures, and  $\text{Co}_2\text{Nb}$  suggest that Co self-diffusion in  $\text{Co}_2\text{Nb}$  occurs by exchange with vacancies.

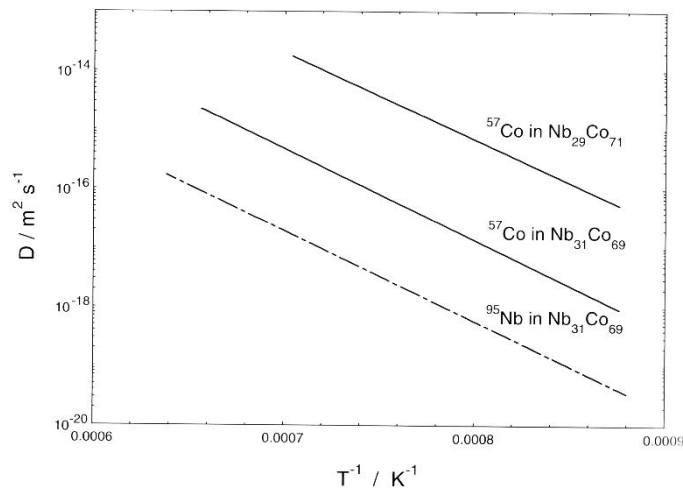


**Fig. 36** Self-diffusion of Co and Nb in the cubic Laves phase  $\text{Co}_2\text{Nb}$ . From [10] according to *Denkinger and Mehrer* [26].

## Acknowledgements

The author is grateful to several former PhD students and coworkers at the author's former group in Münster who contributed with their studies: Ch. Herzig, S. Divinski, Anja Gide, M. Eggersmann, S. Peteline, M. Salamon, M. Denking, and W. Sprengel. The author himself benefitted from a sabbatical stay in the group of Graeme Murch and Irina Belova at the University of Newcastle, Australia.

## References

- [1] T. Graham, *Philos. Mag.* **2**, 175, 222, 351 (1833)
- [2] R. Brown, *Edin. J. Sci.* **1**, 314 (1829)
- [3] A. E. Fick, *Annalen der Physik und Chemie* **94**, 59 (1855); A. E. Fick, *Philos. Mag.* **10**, 30 (1855)
- [4] W. C. Roberts-Austen, *Phil. Trans. of the Royal Society A* **187**, 383 (1996)
- [5] J. Groh, G. von Hevesy, *Annalen der Physik* **65**, 216 (1921).
- [6] A. Einstein, *Annalen der Physik* **19**, 371 (1905).
- [7] J. I. Frenkel, *Z. Physik* **35**, 652 (1928)
- [8] C. Wagner, W. Schottky, *Z. Phys. Chem. B* **11**, 163 (1930)
- [9] A. D. Smigelskas, E.O. Kirkendall, *Trans. AIME* **171**, 130 (1947)
- [10] H. Mehrer, *Diffusion in Solids -- Fundamentals, Methods, Materials, Diffusion-controlled processes*, Springer Series of Solid State Sciences 155, Springer 2007
- [11] J. R. Manning, *Diffusion kinetics for atoms in crystals*, van Norstrand, Princeton. 1968
- [12] I. V. Belova, G.E. Murch, *Philos. Mag.* **A80**, 1469 (2000); *Philos. Mag. A* **81**, 1749 (2001)
- [13] A. Gude, H. Mehrer, *Philos. Mag. A* **76**, 1 (1996)
- [14] M. Eggersmann, H. Mehrer, *Philos. Mag. A* **80**, 1219 (2000)
- [15] H. Mehrer (Vol. Ed.), *Diffusion in Solid Metals and Alloys*, Landolt-Börnstein, New Series, Group III, Vol. 26, Springer-Verlag, 1990

- [16] G. Alefeld, J. Völkl (Eds.), *Hydrogen in Metals I and II*, Topics in Applied Physics I and II, Vols. 28 and 28, Springer-Verlag, 1978 and 1979
- [17] A. B. Kuper, D. Lazarus, J. R. Manning, C. T. Tomizuka. Phys. Rev. **194**, 1536 (1956)
- [18] Ch. Herzig, S. Divinski, in: *Diffusion in Advanced Technological Materials*. D. Gupta (Ed.), William Andrew, Inc., 2005
- [19] A. Gude, H. Mehrer, Philos. Mag. **A 76**, 1 (1997)
- [20] A. E. Kümmerle, K. Badura, B. Sepiol, H. Mehrer, H.-E. Schaefer, Phys. Rev. **B 52**, R6947 (1995)
- [21] B. Sepiol, G. Vogl, Phys. Rev. Letters **71**, 731 (1995)
- [22] S. Peteline, H. Mehrer, M.-L. Huang, Y. A. Chang, Defect and Diffusion Forum **237-240**, 352 (2005)
- [23] M. Salamon, A. Strohm, T. Voss, P. Laitinen, L. Rihimäki, S. Divinski, W. Frank, L. Räisanen, H. Mehrer, Philos. Mag, **84**, 737 (2004)
- [24] M. Salamon, H. Mehrer, Z. Metallkd. **96**, 833 (2005)
- [25] X.Y. Zhang, W. Sprengel, T.E.M. Staab, H. Inui, H.-E. Schaefer, Phys. Rev. Letters **92**, 158592-1 (2004)
- [26] M. Denking, H. Mehrer, Philos. Mag. **A 80**, 1235 (2000)
- [27] H. Bakker, phys. stat. sol. **28**, 569 (1968)
- [28] K. Maier, H. Mehrer, E. Lessmann, W. Schüle, phys. stat. Sol. (b) **78**, 689 (1976)